Title

February 6, 2023 Türkiye Earthquakes: Ground Motions

Journal

Japanese Geotechnical Society Special Publication, 10(11)

ISSN

2188-8027

Authors

Buckreis, Tristan E
Pretell, Renmin
Sandikkaya, Abdullah
et al.

Publication Date

2024

DOI

10.3208/jgssp.v10.ss-6-04

Peer reviewed

February 6, 2023 Türkiye Earthquakes: Ground motions

Tristan E. Buckreis [i)], Renmin Pretell [ii)], M. Abdullah Sandikkaya [iii)], Özkan Kale [iv)], Aysegul Askan [v)], Scott J. Brandenberg [vi)], and Jonathan P. Stewart [vi)]

i) Postdoctoral Scholar, Department of Civil and Environmental Engineering, University of California, Los Angeles, CA, USA
ii) Assistant Professor, Department of Civil and Environmental Engineering, University of Nevada, Reno, NV, USA
iii) Assistant Professor, Civil Engineering Department, Hacettepe University, Ankara, Türkiye
iv) Associate Professor, Department of Civil Engineering, TED University, Ankara, Türkiye
v) Professor, Department of Civil Engineering, Middle East Technical University, Ankara, Türkiye
vi) Professor, Department of Civil and Environmental Engineering, University of California, Los Angeles, CA, USA

ABSTRACT

The 2023 Türkiye/Syria earthquake sequence includes the February 6 **M**7.8 mainshock followed approximately nine hours later by a **M**7.7 aftershock, and many smaller aftershocks including a **M**6.8 and **M**6.3 on February 6 and 20, respectively. These events occurred in a region near the plate boundary of the East Anatolian Fault, in the proximity of which numerous ground motion recordings sites had been installed north of the Türkiye/Syria border. As a result, the events were well recorded both near the fault and at rupture distances up to 570 km. We describe the available recordings and component-specific data processing performed with the aim of optimizing usable bandwidth. The resulting database includes 310, 351, 291, and 229 usable three-component recordings from the **M**7.8, **M**7.7, **M**6.8, and **M**6.3 events, respectively. We also present source, path, and site metadata that was compiled according to uniform protocols. Comparisons to a global ground motion model (GMM) for active tectonic regions and a local, Türkiye-specific model demonstrate the existence of complex path effects that result in relatively poor fits between the GMMs and observed data at large distances (generally R_{JB} > 200 km). Under-predictions at some stations may be influenced by directivity and/or basin effects that affect the ground motions but that are not accounted for directly in the GMMs. We also present analysis of spatial variability of peak ground acceleration for the **M**7.8 mainshock. A residual map produced from this analysis demonstrates that the global GMM over-predicts on the Anatolian block and under-predicts on the Arabian block, further supporting the existence of complex attenuation features in the region.

Keywords: earthquake, ground motions, ground motion models, spatial variability

1 INTRODUCTION

The 2023 Türkiye/Syria earthquake sequence occurred in a region known to have active faults and that was extensively instrumented north of the Türkiye/Syria border. The events were well recorded both near the fault and at distances up to 570 km. This paper describes available recordings as of the present date (August 2023); manual, component-specific data processing that was performed to optimize usable bandwidth; metadata compilation according to uniform protocols; data comparisons to a global ground motion model (GMM) for active tectonic regions and a local, Türkiye-specific model; and analysis of spatial variability of peak ground acceleration (PGA) for the **M**7.8 mainshock.

Several previous ground motion compilations have been presented since the Feb. 6 2023 mainshock (Baltzopoulos et al. 2023; Garini and Gazeta 2023; Gülerce et al. 2023; Kale et al. 2023), and the work presented in this paper updates the work presented in Chapter 3 (Buckreis et al., 2023b) of the EERI-GEER report on this event (Cetin et al. 2023). This work is different from other previous efforts for several reasons, including the use of later-released data from the Disaster and Emergency Management Authority (AFAD) network that corrects errors from earlier releases, the application of NGA protocols for data processing and metadata compilation, and the presentation of data for four events that were of primary interest to reconnaissance teams (Feb. 6 **M**7.8 mainshock and Feb. 6 **M**6.8, Feb. 6 **M**7.8, and Feb. 20 **M**6.3 aftershocks). The data compiled in the present work was compiled for use by reconnaissance teams (Cetin et al. 2023), researchers engaged in Next Generation Attenuation (NGA) projects, and other interested researchers (Buckreis et al. 2023a). This paper presents ground motion data for all four events, however the analyses discussed focus on the Feb. 6 **M**7.8 mainshock.

2 GROUND MOTION DATA AND METADATA

Ground motion data for the Feb. 2023 Türkiye/Syria earthquake sequence is available from seismic networks operating mainly in Türkiye and Cyprus. AFAD in Türkiye operates the Turkish National Strong Motion Network (TNSMN) and the Turkish National Seismic Network (TNSN). The TNSMN is a strong motion network, consisting mainly of accelerometers, while the TNSN are mainly broadband seismometers. TNSMN and TNSN station locations are typically distinct, with only a few collocated stations. These networks produced the majority of recordings from the earthquake sequence, including all of the near-fault records shown in Fig. 1. The principal additional network is the Kandilli Observatory and Earthquake Research Institute, which operate stations mainly in northern parts of Türkiye.

2.1 Sources of ground motion data

Raw (unprocessed) waveforms for each event were obtained from the Earthquake Data Center System of Türkiye (TDVMS; https://tdvms.afad.gov.tr/) and the Incorporated Research Institutions for Seismology (IRIS; Trabant et al. 2012). Data were initially screened to remove duplicate records. The current dataset was downloaded in late March, to obtain unprocessed and baseline-uncorrected records not previously available. An initial visual review was performed to identify and remove records with non-usable data, which include noise-dominated, unclear event signal, early termination, late trigger, instrument malfunction, and spike records.

Many of the recordings from the **M**7.8 event exhibited early termination, likely a result of power failure during the strong shaking. Ground shaking exceeded the upper amplitude limit of most seismometers (instrument code “H”) during the **M**7.8 and **M**7.7 events, so recordings for these events are mostly from accelerometers (instrument code “N”). Unfortunately, there were no usable recordings near Gölbaşı, Şekeroba, and Çelikhan and few near İskenderun and Kahramanmaraş for the **M**7.8 and **M**7.7 events. Few usable records were obtained in the source regions for the **M**6.8 and **M**6.3 aftershocks (near Türkoğlu and Antakya, respectively). At the time of writing, a total of 310, 351, 291, and 229 usable records at stations as far as 570 km, 536 km, 541 km, and 500 km were identified for the **M**7.8, **M**7.7, **M**6.8, and **M**6.3 events, respectively.

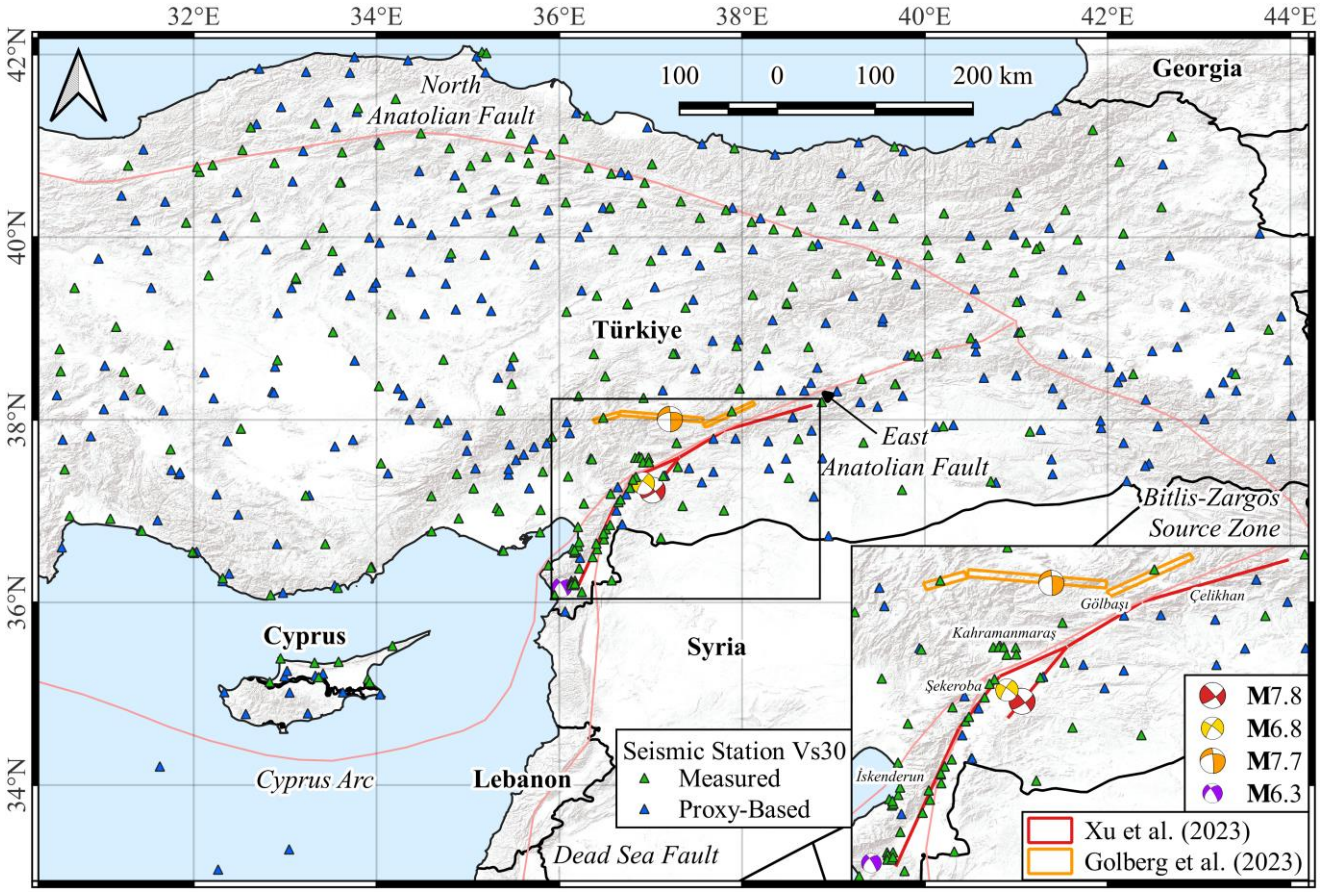

Fig. 1. Map of Türkiye depicting locations and focal mechanisms of **M**7.8, **M**6.8, **M**7.7, and **M**6.3 earthquakes, and seismic stations that recorded usable ground motion data. Surface projections of finite-fault representations for the **M**7.8 and **M**7.7 earthquakes represented by red and orange polygons, respectively. Sites with V_{S30} assigned from measured V_S profiles or from proxy-based models shown by green and blue triangles, respectively.

2.2 Signal processing

Each of the three-component records were processed individually according to standard protocols developed during NGA projects (e.g., Goulet et al. 2021). The procedure consists of applying a baseline correction and high- (and sometimes low-) pass Butterworth filters in the frequency domain. Corner frequencies are selected by visual inspection of the Fourier amplitude spectra (FAS), ratio of the signal-to-noise (SNR), and reasonableness of the displacement time-series. The lowest high-pass corner frequency that satisfies a minimum SNR threshold and produces a reasonable displacement time-series is selected.

This procedure removes any static displacement that might otherwise be present in near-field records, which is the case for records within ~40-70 km of the **M**7.8 and **M**7.7 events. Processing that includes preservation of the fling is not presented in this paper. When using standard processing that does not allow for permanent displacement with records for which such displacements are present, unique challenges arise in the selection of high-pass corner frequencies, $f_{c,HP}$. The difficulty is well illustrated by the TK 4615 (north component) record in Fig. 2, where the different panels show acceleration, velocity, and displacement. This station is located about 0.7 km from the **M**7.8 rupture.

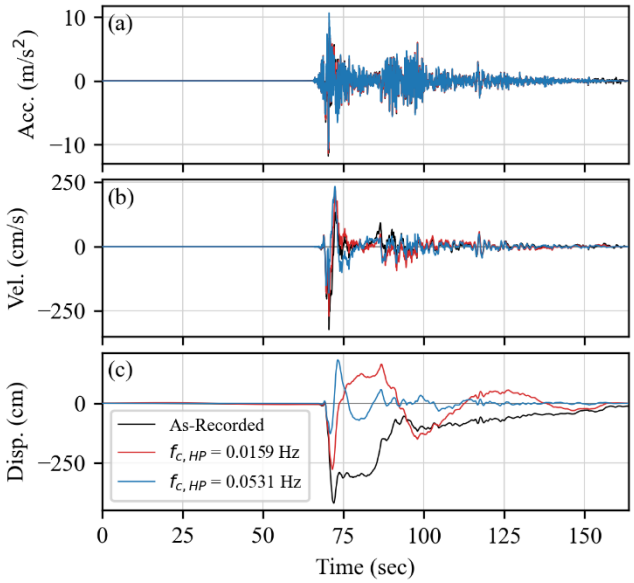

Fig. 2. Example time-series plot illustrating sensitivity of high-pass corner selection for the north component of station TK 4615 from the M7.8 mainshock: (a) acceleration, (b) velocity, and (c) displacement. The peak ground acceleration (PGA) for 0.0159 and 0.0531 Hz high-pass corner frequencies are both 10.66 m/s^2.

In each panel, time series are shown for the unprocessed record, and the record subjected to a relatively modest high-pass filter ($f_{c,HP}$ = 0.016 Hz) that preserves much of the low-frequency energy and a more aggressive high-pass filter ($f_{c,HP}$ = 0.053 Hz). These filter corners were selected considering different objectives: (1) the relatively modest filter ($f_{c,HP}$ = 0.016 Hz) aimed to preserve the velocity pulse between 68 and 75 s, which is associated with the downward (negative displacement) fling step; (2) the more aggressive filter ($f_{c,HP}$ = 0.053 Hz) aimed to remove long-period displacement wobble that occurs when the pulse features are preserved. An alternative way to remove the long-period features would be to fit a velocity pulse function and subtract it from the recording (Shahi and Baker 2014).

As illustrated in Fig. 2, there are different objectives that guide the selection of $f_{c,HP}$ in the present context. The first approach has the advantage of preserving an important component of the ground motion (velocity pulse) but the disadvantage of artificial displacement wobble, while the second approach removes these features. It is not possible to preserve the velocity pulse and obtain reasonable displacements. These considerations affect 44 and 11 ground motions from the **M**7.8 mainshock and the **M**7.7 aftershock, respectively, based on visual assessments during record processing. When processing near-field records in the present work, we chose to prioritize preservation of the velocity pulse over the reasonableness of the displacements.

2.3 Source and Path Metadata

Source metadata are assigned using NGA protocols (e.g., Goulet et al. 2021). Multiple finite fault models (FFMs) for the **M**7.8 and **M**7.7 events are available. We follow criteria from Contreras et al. (2022) to select preferred-FFMs for each event. Accordingly, we adopt the FFM described by Xu et al. (2023) as-published for the **M**7.8 event, and trim the FFM described by Golberg et al. (2023) for the **M**7.7 event. These FFMs were selected because they were developed with consideration of different types of data (e.g., global teleseismic waveforms, local seismic data, and permanent crustal displacements), and produce rupture locations compatible with observed surface rupture (Kozaci et al. 2023). Simulations are used to develop rupture surfaces for the **M**6.8 and **M**6.3 events, as outlined Contreras et al. (2022). Source-to-site distances are evaluated using these finite rupture surfaces.

2.4 Site Metadata

Time-averaged shear wave velocity in the upper 30 m of the site (V_{S30}) values were compiled for each distinct site. The AFAD website reports V_{S30} values computed from V_S profiles measured using geophysical techniques (MASW and ReMi) for 234 of the stations, as shown in Fig. 1. V_{S30} values at 24 of those stations (TK 0125, TK 0201, TK 0603, TK 1201, TK 2401, TK 2518, TK 3113, TK 3116, TK 3133, TK 3143, TK 3144, TK 3301, TK 3801, TK 4614, TK 4628, TK 5001, TK 5201, TK 5505, TK 5508, TK 5801, TK 5804, TK 6004, TK 6302, and TK 6901) were updated relative to those on the AFAD website. These updates were motivated by some errors (specifically, inconsistencies with the 1D

layered earth models at some stations). The corrections of these errors adjusted the V_S profiles and the V_{S30} values.

Proxy-based V_{S30} models were used to assign V_{S30} values at locations without site characterization data. The Zhou (2023) proxy model based on topographic slope and kriging interpolation of V_{S30} values computed from measured V_S profiles and the Yilmaz et al. (ongoing project) geology- and topography-based models are used at stations within Türkiye. Outside of Türkiye, V_{S30} values are assigned using the topographic slope-based proxy model proposed by Wald and Allen (2007).

3 COMPARISONS OF DATA TO GLOBAL AND LOCAL GROUND MOTION MODELS

We compare recorded data with the following GMMs for shallow crustal regions: (1) a global model - Boore et al. (2014; hereafter BSSA14) and (2) a Türkiye-specific model by Kale et al. (2015; hereafter KAAH15). The BSSA14 model can be applied with or without regional adjustments of the rate of anelastic attenuation, being relatively low for Türkiye (slower attenuation) and relatively high for Italy (faster attenuation). Without a regional adjustment, the model is considered applicable to California, New Zealand, and Taiwan.

The GMMs provide predictions of ground shaking intensity given **M**, rupture mechanism/style-of-faulting (strike-slip for all events considered), R_{JB}, and V_{S30}. BSSA14 has basin adjustments for iso-surface depths (i.e., $z_{1.0}$), however given that this site parameter is unavailable for the vast majority of sites, we choose not to apply any basin adjustments during this analysis (i.e., the differential depth $\delta z_{1.0} = 0$).

To evaluate the performance of the BSSA14 (global and Türkiye-regionalized) and the KAAH15 GMMs, we compute total residuals (R_{ij}), considering the appropriate path and site conditions as follows:

$$R_{ij} = \ln(Y_{ij}) - \ln(y_{ij}) \quad (1)$$

where Y_{ij} is the value of the observed ground motion intensity measure (e.g., PGA) from station i for event j, and y_{ij} is the median GMM prediction. Fig. 3 plots PGA R_{ij} versus distance for both GMMs. Binned means are also shown for R_{ij}, along with their 95% confidence intervals. Only data from free-field sites are shown.

We find that all GMMs fit the observed PGA data reasonably well out to distances of about 100-200 km. The global BSSA14 model fits the data best at distances < 100-200 km, but under-predicts at distances beyond. The Türkiye-regionalization of BSSA14 reduces the anelastic attenuation compared to the global model, which results in significant over-prediction at far distances (R_{JB} > 80 km). The KAAH15 model similarly over-predicts PGA in the far-field because the model does not include terms to account for anelastic attenuation effects.

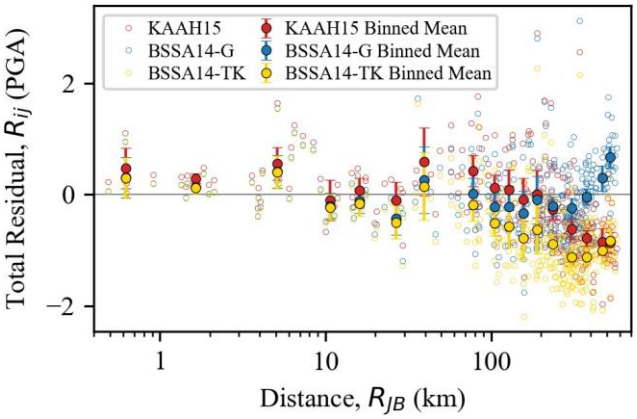

Fig. 3. Peak ground acceleration (PGA) total residuals versus distance (R_{JB}) for the **M**7.8 mainshock. Residuals computed for the KAAH15, global-BSSA14 (BSSA14-G), and Türkiye – regionalized BSSA14 (BSSA14-TK) GMMs.

The trends shown in Fig. 3 suggest the existence of complex path effects that result in relatively poor fits between the GMMs and observed data at large distances (generally R_{JB} > 200 km). The Turkish data considered in the development of the regionalized BSSA14 model was mainly from the northern part of Türkiye, near the North Anatolian Fault. The present earthquake sequence occurred in southern-Türkiye, near the interface of the Anatolian and Arabian plates. These results suggest that different crustal properties are encountered in the different parts of Türkiye, which is likely a consequence of the different crustal blocks. For these reasons, we prefer the global BSSA14 model for the analyses presented subsequently.

4 SPATIAL ANALYSIS

Correlation models are developed to characterize the spatial pattern of PGA within-event residuals (δW_{ij}) for the **M**7.8 mainshock. To this end, δW_{ij} for PGA are computed for the BSSA14 (global) model as:

$$\delta W_{ij} = R_{ij} - \eta_{E,i} \quad (2)$$

where $\eta_{E,i}$ represents the event term, estimated as the average of all R_{ij} within an R_{JB} = 200 km (this distance range approximately envelopes stations with unbiased GMM predictions). The δW_{ij} values are then normalized by their standard deviation ϕ_j:

$$\delta \grave{W}_{ij} = \frac{\delta W_{ij}}{\phi_j} \quad (3)$$

The $\delta \grave{W}_{ij}$ values are used to develop the correlation models. In this work, we apply correlation models that account for between-station closeness in Euclidean distance (ρ_E) and azimuthal distance (ρ_A) (Bodenmann et al. 2023):

$$\rho_{EA}(d_E, \gamma_E) = \rho_E(d_E, \gamma_E) \cdot \rho_A(d_A) \quad (4)$$

where:

$$\rho_E(d_E, \gamma_E) = exp\left[-1 \cdot \left(\frac{d_E}{\ell_E}\right)^{\gamma_E}\right] \quad (5)$$

$$\rho_A(d_A) = \left(1 + \frac{d_A}{\ell_A}\right) \cdot \left(1 - \frac{d_A}{180}\right)^{\frac{180}{\ell_A}} \quad (6)$$

where d_E is the Euclidean distance (km) between two seismic stations, γ_E is a model coefficient ℓ_E is the Euclidean corelation length (km), d_A is the azimuthal angle (degrees) between two seismic stations, and ℓ_A is the azimuthal correlation angle (degrees).

Bayesian inference is used to estimate the model coefficients ℓ_E, γ_E, and ℓ_A. A Bayesian approach allows for establishing prior distributions for the model parameters and updating them using the available ground motion data. This avoids potentially spurious models that could result from a purely data-driven least-squares regression approach. In addition, Bayesian inference allows for the estimation of multiple models that altogether better capture the model uncertainty. A set of one thousand model coefficients are sampled from the posterior joint distributions, resulting in 1000 correlation models. The maximum a posteriori (MAP) model, i.e., the model most supported by the data, is also estimated and used to develop a δW_{ij} map of PGA for the **M**7.8 mainshock. The correlation models are presented in Fig. 4.

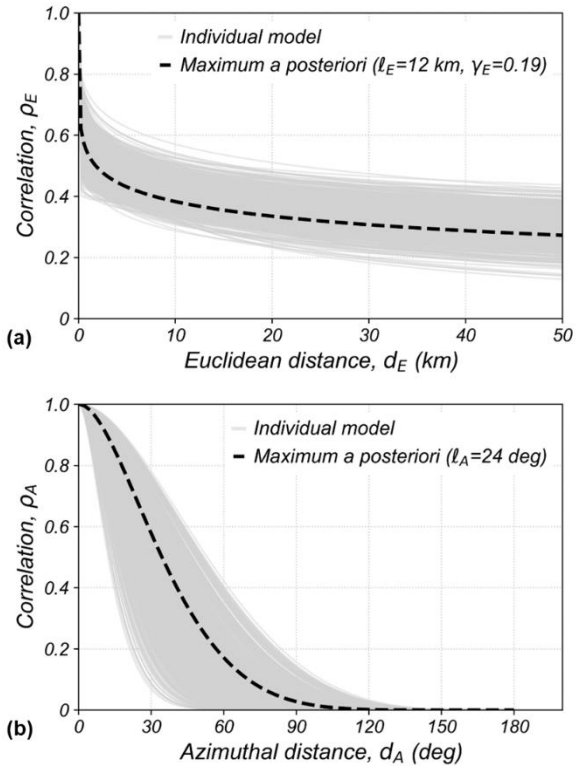

Fig. 4. Bayesian correlation models for peak ground acceleration (PGA) within-event residuals from the **M**7.8 mainshock. (a) Correlation models dependent on the Euclidean distance (ρ_E), and (b) Correlation models dependent on the azimuthal distance (ρ_A).

Ordinary Kriging is used to estimate the mean δW_{ij} and the associated standard deviation of the interpolation error at any given location. The interpolation errors, estimated as part of the Kriging step, are due to the closeness of a given unsampled location to the closest seismic station. Locations close to a seismic station have lower standard deviation, while locations further away from seismic stations have higher standard deviations. The standard deviation of the interpolation error at seismic stations is zero.

Fig. 5 presents the derived δW_{ij} map that demonstrates spatial patterns of the PGA residuals. The colorization in Fig. 5 indicates areas of weaker- and stronger-than-average ground motions (blue and red, respectively). Interestingly, there is a rather clear distinction between areas predominated by blue and red shading. Keeping in mind that that the **M**7.8 mainshock ruptured the East Anatolian Fault which serves as the boundary between the Anatolian and Arabian plates, we generally find negative residuals (blue) on the Anatolian plate and positive residuals (red) on the Arabian plate. These results suggest that the global BSSA14 model over-predicts on the Anatolian plate and under-predicts on the Arabian plate.

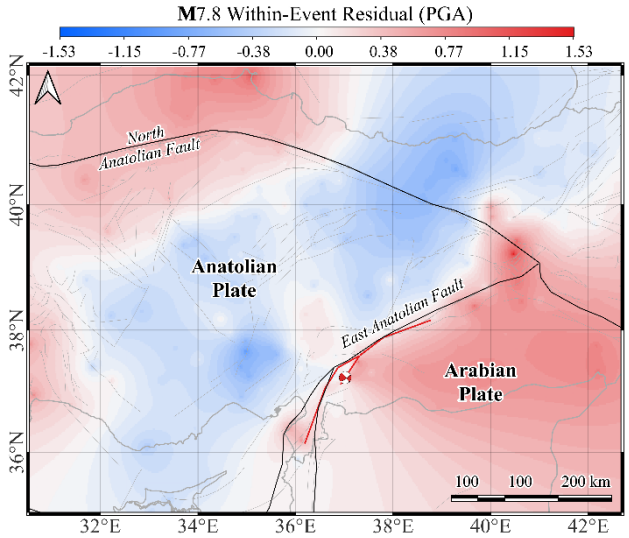

Fig. 5. Mean within-event residual for peak ground acceleration (PGA) from the **M**7.8 mainshock developed using the maximum a posteriori correlation models. Blue and red shading indicate areas of weaker- and stronger-than-average ground motions, respectively.

The results shown in Fig. 5 are fairly consistent across the other events (as well as for other intensity measures, such as peak ground velocity and pseudo-spectral accelerations at different oscillator periods). These findings further reinforce the hypothesis of tectonic block-dependent anelastic attenuation in southern Türkiye, as well as provide evidence that different crustal properties are encountered in the two parts of Türkiye, that are likely a consequence of the different crustal blocks. It is noteworthy that at closer

distances where path effects are dominated by geometric spreading, the global ergodic model is effective.

5 SUMMARY

The Feb. 2023 Türkiye/Syria earthquake sequence is a once-in-a-century catastrophe, whose repercussions will have a lasting effect on the region. This paper presents the ground motion data from these events, which will be influential for future GMM development efforts and used as validation data for ground motion simulations, among other applications. Comparisons of ground motions from the Feb. 6 **M**7.8 mainshock to global and local GMMs suggest the existence of complex path effects in the region, uncaptured by the existing models. Spatial analysis of the PGA residuals suggests that the complex attenuation features are likely related to differences in crustal properties between the Anatolian and Arabian plates.

REFERENCES

Baltzopoulos, G., Baraschino, R., Chioccarelli, E., Cito, P., and Iervolino, I. (2023): Preliminary Engineering Report on Ground Motion Data of the Feb. 2023 Turkey Seismic Sequence, Consortium of Italian Universities, Feb 24 2023.

Bodenmann, L., Baker, J.W., and Stojadinovic, B. (2023): Accounting for path and site effects in spatial ground-motion correlation models using Bayesian inference, *Natural Hazards and Earth System Sciences*23:2387–2402.

Boore, D.M., Stewart, J.P., Seyhan, E., and Atkinson, G.M. (2014): NGA-West2 equations for predicting PGA, PGV, and 5%-Damped PSA for Shallow Crustal Earthquakes, *Bulletin of the Seismological Society of Am*erica 30(3): 1057-1085.

Buckreis, T.E**.**, Güryuva, B., İçen, A., Okçu, O., Altindal, A., Aydin, M.F., Pretell, R., Sandikkaya, M.A., Kale, O., Askan, A., Brandenberg, S.J., Kishida, T., Akkar, S., Cetin, O., Bozorgnia, Y., and Stewart, J.P. (2023a): Chapter 3: Ground Motions, *in February 6, 2023 Türkiye: Report on Geoscience and Engineering Impacts, Report GEER-082*, GEER Association.

Buckreis, T., Güryuva, B., İçen, A., Okcu, O., Altindal, A., Aydin, M., Pretell, R., Sandikkaya, S., Kale, O., Askan, A., Brandenberg, S., Kishida, T., Akkar, S., Bozorgnia, Y., and Stewart, J. (2023b): *Ground Motion Data from the 2023 Türkiye-Syria Earthquake Sequence*, DesignSafe-CI. https://doi.org/10.17603/ds2-t115-bk16 v3

Cetin, K.O., Bray,J.D.,Frost, D.J., Hortacsu,A.,Moss,R.E.S., and Stewart, J.P. (2023):February 6, 2023 Türkiye Earthquakes: Report on Geoscience and Engineering Impacts, *Report GEER-082*, GEER Association, 382 pages.

Contreras, V., Stewart, J.P., Kishida, T., Darragh, R.B., Chiou, B.S.J., Mazzoni, S., Youngs, R.R., Kuehn, N.M., Ahdi, S.K., Wooddell, K., Boroschek, R., Rojas, F., and Ordenes, J. (2022): NGA-Sub source and path database, *Earthquake Spectra* 38(2): 799–840.

Garini, E. and Gazetas, G. (2023): The Turkey-Syria Mw 7.8 Earthquake of February 6 2023, Recorded Accelerograms and their Response Spectra, National Technical University, Athens.

Gülerce, Z., Askan, A., Kale, O., Sandıkkaya, A., Işı, N.S., İlhan, O., Can, G., Ilgaç, M., Ozacar, A.A., Sopacı, E., Çen, K.O., Akbaş, B., Alndal, A., Guryuva, B., Kanun, O., Albayrak, K., Muratoglu, G., Okcu, O.S., Icen, A., and Aydin, M.F. (2023): Chapter 4: Preliminary Analysis of Strong Ground Moon Characteriscs, February 6, 2023 Kahramanmaraş-Pazarcik (Mw=7.7) and Elbistan (Mw=7.5) Earthquakes, Report by Middle Eastern Technical University.

Kale, Ö., Akkar, S., Ansari, A., and Hamzehloo, H. (2015): A ground-moon predictive model for Iran and Turkey for horizontal PGA, PGV, and 5% damped response spectrum: Investigation of possible regional effects, *Bulletin of the Seismological Society of Am*erica 105(2A): 963 - 980.

Kale, Ö., Sandıkkaya, M.A., Akbaş, B., Albayrak, K., Alndal, A., Askan, A., Aydın, M.F., Can, G., Çen, K.O., Gülerce, Z., Güryuva, B., Ilgaç, M., Işık, N.S., İçen, A., İlhan, O., Kanun, O., Muratoğlu, G., Okçu, O.S., Özacar, A.A., and Sopacı, E. (2023): Analysis for Strong Ground Moon Characteriscs from the 6 February 2023 Kahramanmaraş-Türkiye Earthquakes: Pazarcık Mw 7.8 and Elbistan Mw 7.7, *Bulletin of Earthquake Engineering*

Golberg, D.E., Taumaz, T., Reitman, N.G., Hatem, A.E., Yolsal-Çevikbilen, S., Barnhart, W.D., Irmak, T.S., Wald, D.J., Öcalan, T., Yeck, W.L., Özkan, B., Thompson-Jobe, J.A., Shelly, D.R., Thompson, E.M., DuRoss, C.B., Earle, P.S., Briggs, R.W., Benz, H., Erman, C., Doğan, A.H., and Altuntaş, C. (2023): Rapid characterization of the February 2023 Kahramanmaraş, Türkiye, earthquake sequence, *The Seismic Record* 3(2): 156-167

Goulet C.A., Kishida, T., Ancheta, T.D., Cramer, C.H., Darragh, R.B., Silva, W.J., Hashash, Y.M.A., Harmon, J., Parker, G.A., Stewart, J.P., and Youngs R.R. (2021): PEER NGA-East database, *Earthquake Spectra* 37(1): 1331-1353.

Shahi, S.K. and Baker, J.W. (2014): An efficient algorithm to identify strong velocity pulses in multi-component ground moons, *Bulletin of the Seismological Society of Am*erica 104(5): 2456–2466.

Trabant C., Hutko, A.R., Bahavar, M., Karstens, R., Ahern, T., and Aster, R. (2012): Data Products at the IRIS DMC: Stepping Stones for Research and Other Applications, *Seismological Research Letters* 83(5): 846–854.

Wald, D.J. and Allen, T.I. (2007): Topographic slope as a proxy for seismic site conditions and amplification, *Bulletin of the Seismological Society of America* 97(5): 1379 - 1395.

Xu, L., Mohanna, S., Meng, L., Ji, C., Ampuero, J.P., Yunjun, Z., Hasnain, M., and Chu, R. (2023): The 2023 Kahramanmaras, Turkey earthquake: A multi-segment rupture in a millennium supercycle, Preprint (1). https://doi.org/10.21203/rs.3.rs-2747911/v1

Yilmaz et al. (ongoing project): Production of GIS-based predicted-Vs30 maps at a scale of Turkey by using geological and topographical digital maps, Project ID; AFAD-UDAP-Ç-20-01, 2020-2023.

Zhou, J. (2023): VS30 data of Turkey AFAD strong-moon network stations and VS30 map of Turkey and adjacent area related to the Feb. 2023 Turkey Earthquake Sequence. doi: 10.13140/RG.2.2.24389.12007.